Fig. 3. Orbital radii of the Jovian and Neptunian satellites line up with the orbital radii of the Uranian satellites after Eqs. (1) and (2) are used to transform the Jovian and Neptunian orbital radii.

Figure 3

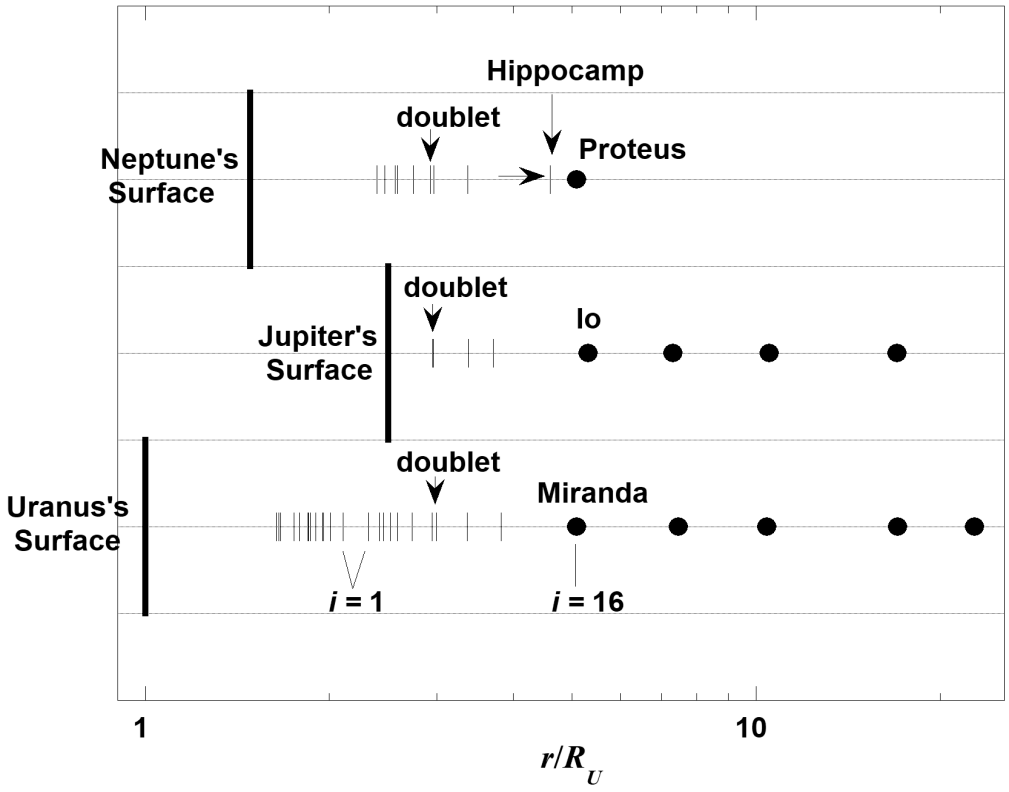

In Fig. 3 the large dots in the Uranian line graph correspond to Uranus's major satellites. In the Jovian graph large dots represent the Galilean satellites. In the Neptunian graph Proteus is by far the most massive regular satellite as seen in Table 3. We observe the most massive satellites exist at and beyond orbital radii for which $i = 16$. Later discussions in the present investigation will link distributions of satellite orbital radii to protosatellite disks. Fig. 3 and this linkage indicates that massive satellites are created in similar regions of protosatellite disks.

2.2.a. A Smooth Relationship Exists Between Photon Energies in the H_2 Spectrum and the Orbital Radii of Uranian Satellites

The linearity of the graphs in Figs. 1 and 2 suggests a common mechanism creates the primordial rings around Uranus, Jupiter and Neptune which evolve into satellites. The present investigation explores the possibility that photons corresponding to molecular hydrogen (H_2) lines interact with molecules in the protosatellite disks of Uranus, Jupiter and Neptune and through the SRMA mechanism initiate the creation of primordial rings. Such lines are prominent in the spectra of nebulae. Draine and Bertoldi (1996) have modeled the spectrum of the reflection nebula NGC 2023, and Martini et al. (1999) have observed the spectra of four reflection nebulae including NGC 2023. In both of these investigations, the

large spectral peaks in the range 5560 – 4290 cm^{-1} (1.80 – 2.33 μm) all correspond to S-branch transitions (lines) in the H_2 spectrum. The segment of the H_2 spectrum that we focus on is shown in Fig. 1 of Martini et al. (1999) which is a model spectrum for the reflection nebulae they observed. Fig. 4 in the present investigation is a similar model spectrum developed using photon energies (E_p's) and spectral intensities (I's) from Black and van Dishoeck (1987). E_p's in Fig. 4 and throughout this paper are in wave numbers (cm^{-1}). Also in Fig. 4 each index i is associated with a particular S-branch transition. That is, each i value stands for a particular transition in H_2.

Fig. 4. H_2 S-Branch Spectrum: Starred(*) spectral lines fall outside the range of peaks that affect the Uranian disk or corresponding to intensities that are too low to cause resonance.

Figure 4

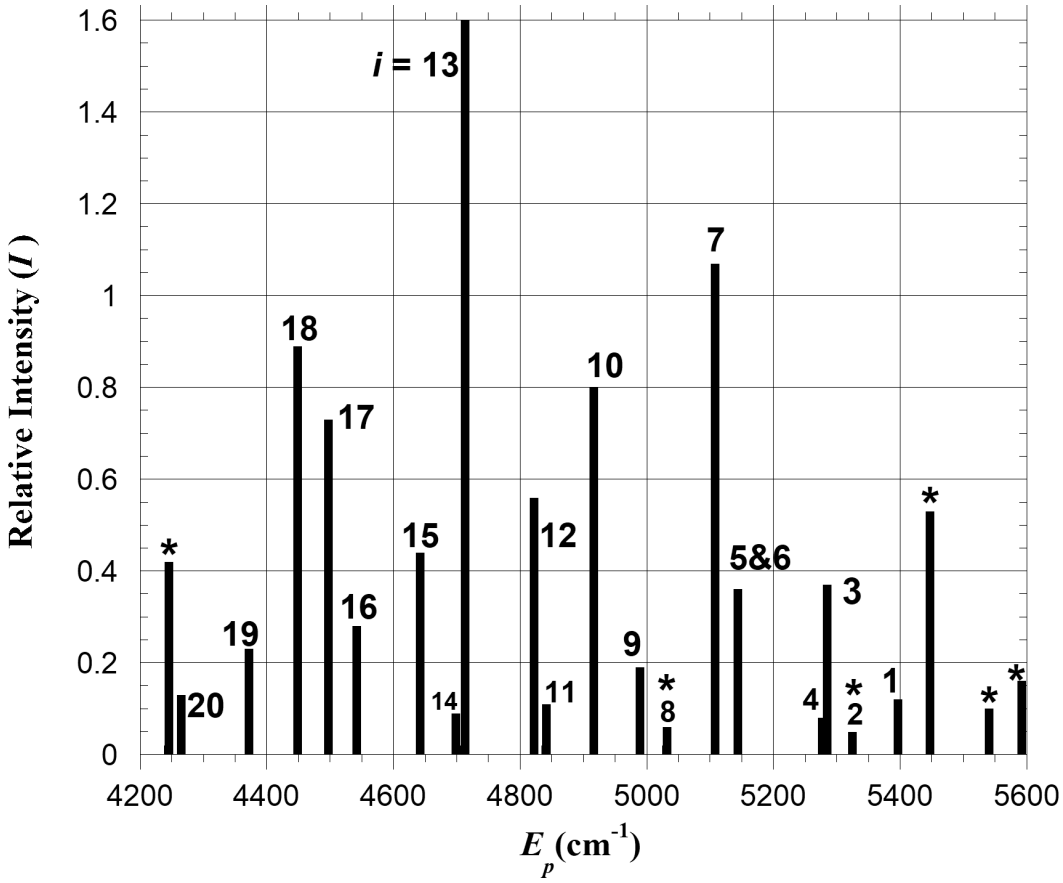

The origin of the photons in the H_2 spectrum that initiate the key SRMA reactions in a disk is not identified in the present investigation. Perhaps they come from H_2 molecules that reside in the the disk. Or perhaps they come from the protosun, presumably a typical T Tauri star. The H_2 spectrum is observed as a component of the overall spectra of T Tauri stars (Beckwith, Gatley, Matthews and Neugebauer 1978, and Herczeg et al. 2006). Furthermore, FUors and EXors (Hartmann, Kenyon and Hartigan 1993) are subclasses of T Tauri's. These objects are characterized by short-lived magnitude changes of up to 6 magnitudes with rise times on the order of months to years (Appenzeller and Mundt 1989, and Herbig 1977). Possibly the protosun in such a short lived state delivers the photons that initiate resonance rings in protoplanetary disks.

Table 4 lists the complete set of regular Uranian satellites and their orbital radii (R_{ui}) in units of the equatorial radius of Uranus. The subscript i is a reminder that each orbital radius depends on an H_2 spectral line or in some cases a close pair of lines. Table 4 also contains data related to the spectral lines mentioned above. Each R_{ui} is paired with a particular value of E_p or a weighted average of two E_p's if two spectral lines are very closely spaced. This particular set of pairings produces a smooth graph of E_p vs R_{ui} which is referred to as a photon energy distribution (PED). The PED has a dip, peak and a long tail as seen in Fig. 5a. The method used for establishing the particular set of pairings (R_{ui}, E_p) in Table 4 is given in section 2.2.b. Later, more credence is given to the concept of the PED when it is linked to the temperature distribution (TD) of the Uranian protosatellite disk.

Fig. 5a. The complete PED in the Uranian protoplanetary disk

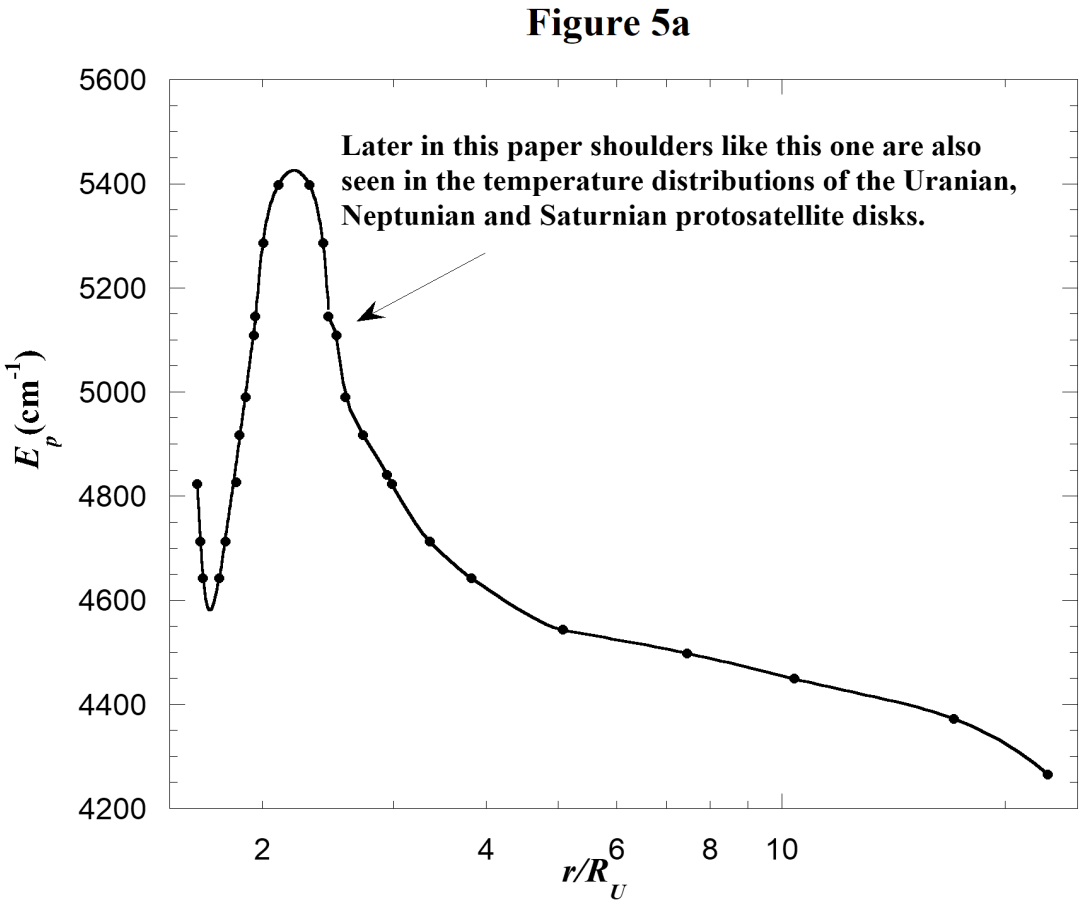

Table 4. H_2 Transitions and their associated photon energies (E_P's) and relative spectral intensities (I's) associated with Uranian satellite orbital radii (R''_{ui}, R'_{ui} and R_{ui})

i	H_2 Transition[a]	E_P(cm^{-1})[a]	I [a]		E_P's for Figs. 5a ,5b and 5c	Uranian Satellite	(R_{ui}'' or R'_{ui})[b]
11	**(3,2) S(5)**	**4841**	**0.11**				
				→	**4826**[c]	**Ring 6**	**1.637**
12	**(2,1) S(3)**	**4823**	**0.56**				
13	**(1,0) S(1)**	**4713**	**1.6**				
				→	**4712**[c]	**Ring 5**	**1.652**
14	**(3,2) S(4)**	**4699**	**0.09**				
15	(2,1) S(2)	4642	0.44		4642	Ring 4	1.666
15	(2,1) S(2)	4642	0.44		4642	Ring α	1.750
14	**(3,2) S(4)**	**4699**	**0.09**				
				→	**4712**[c]	**Ring β**	**1.786**
13	**(1,0) S(1)**	**4713**	**1.6**				
12	**(2,1) S(3)**	**4823**	**0.56**				
				→	**4826**[c]	**Ring η**	**1.834**
11	**(3,2) S(5)**	**4841**	**0.11**				
10	(1,0) S(2)	4917	0.8		4917	Ring γ	1.863
9	(2,1) S(4)	4990	0.19		4990	Ring δ	1.900
8	(9,7) S(0)[d]	5032	0.06				
7	(1,0) S(3)	5108	1.07		5108	Cordelia	1.948
6	**(2,1) S(5)**	**5142**	**0.25**				
				→	**5144**[c]	**Ring λ**	**1.957**
5	**(9,7) S(1)**	**5147**	**0.11**				
4	**(2,1) S(6)**	**5278**	**0.08**				
				→	**5285**[c]	**Ring ε**	**2.006**
3	**(1,0) S(4)**	**5286**	**0.37**				
2	(9,7) S(3)[d]	5325	0.05				
1	(2,1) S(7)	5397	0.12		5397	Ophelia	2.105

continued

Table 4 continued

i	H_2 Transition[a]	E_P(cm^{-1})[a]	I[a]		E_P's for Fig 5	Uranian Satellite	R_{ui}[b]
1	(2,1) S(7)	5397	0.12		5397	Bianca	2.316
2	(9,7) S(3)[d]	5325	0.05				
3	**(1,0) S(4)**	**5286**	**0.37**				
				→	**5285**[c]	**Cressida**	**2.418**
4	**(2,1) S(6)**	**5278**	**0.08**				
5	**(9,7) S(1)**	**5147**	**0.11**				
				→	**5144**[c]	**Desdemona**	**2.453**
6	**(2,1) S(5)**	**5142**	**0.25**				
7	(1,0) S(3)	5108	1.07		5108	Juliet	2.520
8	(9,7) S(0)[d]	5032	0.06				
9	(2,1) S(4)	4990	0.19		4990	Portia	2.586
10	(1,0) S(2)	4917	0.8		4917	Rosalind	2.735
11	(3,2) S(5)	4841	0.11		4841	Belinda	2.946
12	(2,1) S(3)	4823	0.56		4823	Perdita	2.990
13	**(1,0) S(1)**	**4713**	**1.6**				
				→	**4712**[c]	**Puck**	**3.365**
14	**(3,2) S(4)**	**4699**	**0.09**				
15	(2,1) S(2)	4642	0.44		4642	Mab	3.824
16	(3,2) S(3)	4543	0.28		4543	Miranda	5.082
17	(1,0) S(0)	4498	0.73		4498	Ariel	7.469
18	(2,1) S(1)	4449	0.89		4449	Umbriel	10.407
19	(3,2) S(2)	4372	0.23		4372	Titania	17.070
20	(4,3) S(3)	4265	0.13		4265	Oberon	22.830

[a]Black van Dishoeck (1987)

[b]NASA (2021)

R''_{ui} refers to orbital radii from Ring 6 to Ring 4.

R'_{ui} refers to orbital radii from Ring α to Ophelia.

R_{ui} refers to orbital radii from Bianca to Oberon.

[c]A bolded E_P is a weighted average of the E_P's on the previous and following lines. The weighting factors are the corresponding I's.

[d]It is not possible to associate this low intensity spectral line with any satellite.

Note that spectral lines appear in Table 4 one to three times because the PED has a dip and a peak in it. Also Fig. 4 shows closely spaced lines corresponding to indices 3&4, 5&6 and 13&14. In these cases a weighted average of E_p's is used with the weighting factors being the corresponding spectral intensities. The closely spaced lines with indices 11&12 have their E_p's averaged for ring 6 and ring η (ring η is known to have two components (French et al. 1991)). But they are resolved for the "doublet" Belinda and Perdita. Two spectral lines with indices 2 and 8 are omitted from the analysis because they have low relative intensity as is indicated in Table 4 and Fig. 4 and they cannot be paired with orbital radii. Cupid's orbital radius is also omitted from the analysis as previously mentioned.

2.2.b. The Determination of the Relationship Between E_p Values and Orbital Radii Given in Table 4 and Figs. 5a & 5b

The following are the steps taken to develop the (PED) discussed in the previous subsection. By trial and error it is determined that if the R_{ui}'s for rings α, β, η, γ, δ and satellite Cordelia are paired with E_p's corresponding to i 's 15, 14&13, 12&11, 10, 9 and 7 respectively as in Table 4, then a plot of E_p vs R_{ui} is well fitted by a straight line shown by the straight dashed portion of the curve in Fig. 5b. The point for ring η is noticeably the furthest away from the straight line fit. It is interesting that the radius of ring η is very near the 3:2 Inner Lindblad Resonance of the satellite Cressida (Chancia et al. 2017). Perhaps the radius of ring η has been affected by its interaction with Cressida.

Fig. 5b. The photon energy distribution from Ring 6 to Desdemona

Figure 5b

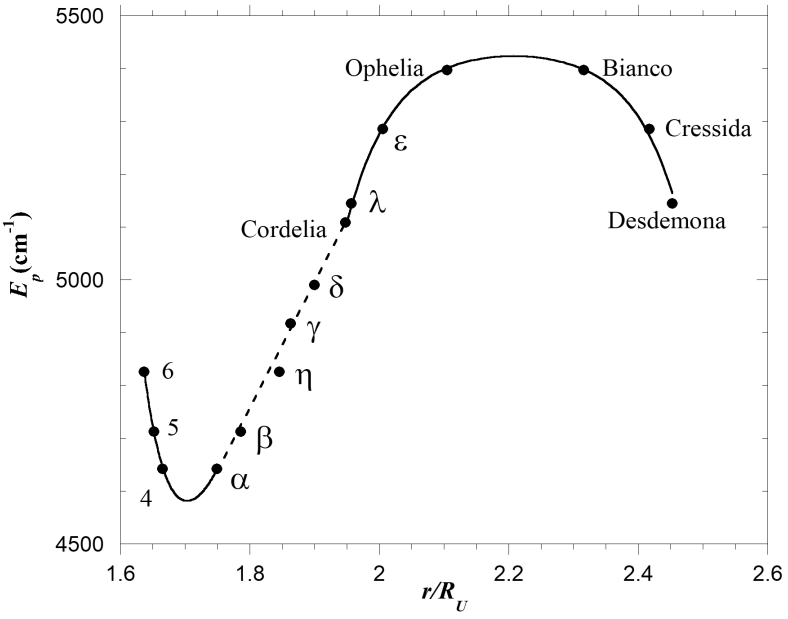

When we pair rings 6, 5 and 4 (the three innermost rings) incorrectly with i 's 18, 17 and 16 (which might be the expected inward extension of i 's) a discontinuity is created as seen in Fig. 5c. If instead we use the i 's 12&11, 14&13 and 15 for the three innermost rings a smoothly varying dip becomes apparent as seen in Fig. 5b.

Fig. 5c. The Photon Energy Distribution with Discontinuity

Figure 5c

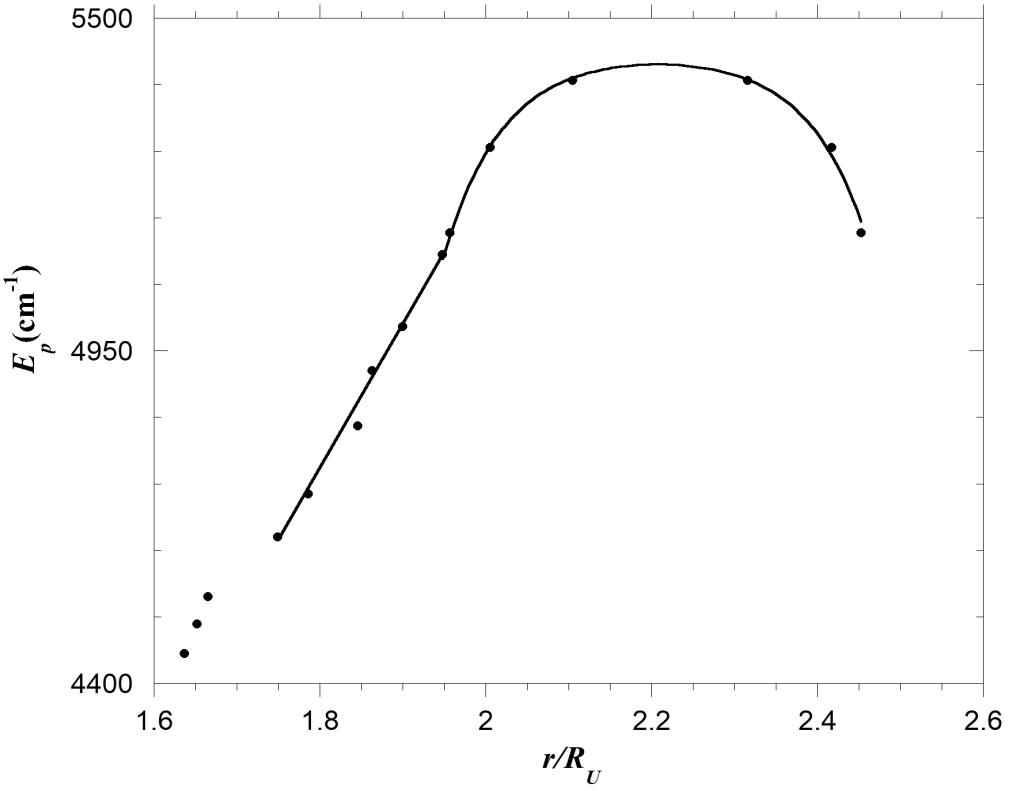

A similar situation occurs for the region from Cordelia to Desdemona in Fig. 5b. If we don't assume a peak occurs there, a discontinuity occurs because of the wide radial gap between Ophelia and Bianca. If we assume a peak, then we find the curve is smoothly varying, symmetric and centered at r/R_U = 2.21 where r is the radial coordinate in units of km. This point is half-way between Ophelia and Bianca as seen in Fig. 5b.

Notice that Bianca is assigned i = 1 just as for Ophelia. In Table 4 and Fig. 5a, the rest of the PED beyond Bianco does not have any more dips or peaks and each satellite in turn is assigned an ever increasing i or pair of i 's all the way out to i = 20 for Oberon the last regular satellite.

2.3.a. Comparing the PED in Figure 5a to TD's of the Solar Nebula

Given that processes which govern the behavior of protosatellite disks and the protoplanetary disk (solar nebula) are similar (Mousis et al. 2002, Mousis 2003, and Mousis and Alibert 2006), we now compare the PED in Figs. 5a to temperature distributions (TD's) calculated by Lin and Papaloizou (1985, hereafter L&P (1985)) for the solar nebula. Fig.18 of L&P (1985) contains two sets of graphs showing midplane TD's of the solar nebula for two different times during what are called upward and downward transition waves. We find the PED in Fig. 5b to be similar in shape to the L&P (1985) solar nebula TD's. Both types of L&P (1985) TD's are peaked and have characteristics similar to those of the PED in Fig. 5a. To the right of the peak in the L&P (1985) TD at the onset of the transition, there is a negatively sloped tail just as in the PED in Fig. 5a. Also, in the L&P (1985) distribution near the end of the downward transition and to the left of the peak, the TD has a dip just as in the PED in Fig. 5a.